# Structure and contact angle of liquid $^4$He droplets on a Cs surface

Francesco Ancilotto, Anna Maria Sartori, and Flavio Toigo
*INFM-Dipartimento di Fisica ''G. Galilei''- Universita' di Padova, via Marzolo 8, I-35131 Padova, Italy*
(Received 8 April 1998)

By using a density-functional approach, we have studied the $T=0$ nonwetting behavior of liquid $^4$He nanodroplets on a Cs surface. The minimum energy structure of the droplets is determined and its dependence upon size is investigated. The comparison with a simple model of droplet adsorption suggests a way to extrapolate our result to the experimentally accessible case of macroscopic droplets. In particular, a value for the contact angle of macroscopically thick droplets, which is an important parameter in wetting phenomena, is predicted. Our calculated value for the contact angle is in semiquantitative agreement with recent experimental observations. [S0163-1829(98)02732-5]

## I. INTRODUCTION

Superfluid $^4$He is an almost universal wetting agent: its liquid in contact with most surfaces spreads to form a continuous film over the surface so that vapor and substrate are never in contact. Alkali metal surfaces represent a striking exception to this general behavior:[1] theoretical calculations[2,3] predicted and subsequent experiments[4–6] confirmed that $^4$He does not wet the surface of Cs. This is a remarkable consequence of the fact that the $^4$He-Cs interaction is much weaker than that between two $^4$He atoms: the hard-core repulsion arising from the very diffuse electron charge surrounding the alkali atom core keeps the $^4$He atom relatively far from it, in a region where the rapidly decaying van der Waals attractive interaction is very small.

The nonwetting behavior of $^4$He on Cs implies that the adsorbed film is always atomically thin at low temperatures and it only becomes macroscopically thick when $T>T_W$, $T_W\sim 2$ K being the wetting temperature for the $^4$He-Cs system.[5] This behavior characterizes the so-called partial wetting of the solid. The low-temperature thin film disappears as $T\to 0$ (''dry'' nonwetting behavior) as reported in Refs. 7 and 8. As a consequence, at very low temperatures, finite amounts of liquid $^4$He on a Cs substrate coalesce to form macroscopic droplets.[9] A three-phase contact line thus exists, where substrate, liquid, and vapor meet. The intersection of a macroscopic droplet profile with the substrate is characterized by the contact angle $\theta$, which depends on temperature: it goes to zero as $T$ approaches $T_W$ and remains zero at all higher temperatures, where the liquid wets the substrate. The contact angle $\theta$ is determined by balancing the forces acting along the contact line and is found to depend on the interfacial tensions $\sigma_{ij}$ between each pair of coexisting phases through the Young-Dupre equation:

$$\cos\,\theta=\frac{\sigma_{sv}-\sigma_{sl}}{\sigma_{lv}}. \tag{1}$$

The subscripts $l$, $v$, and $s$ identify the liquid, vapor, and solid, respectively. As the interfacial tensions vary with temperature,[10] a phase transition[3] from the partial to the complete wetting regime can be induced by raising the temperature over the wetting temperature $T_W$. The observed discontinuity in $d\cos(\theta)/dT$ at $T=T_W$ signals that the wetting transition is first order.[5,11]

Theoretical estimates for the $T=0$ contact angle range from an early value $\theta=95°$ (Ref. 2) to the more recent $\theta=30°$.[12] These estimates are based on the assumption that $\Delta\sigma\equiv\sigma_{sv}-\sigma_{sl}$ is temperature independent, so that $\theta(T=0)$ is given by $\cos\theta(0)=\Delta\sigma/\sigma_{lv}(0)$ with $\Delta\sigma=\sigma_{lv}(T_W)$. However, there is clear experimental evidence that $\sigma_{sl}$ is a strong function of temperature.[8,13] This may raise some questions about the accuracy of the estimates of $\theta$ that are based on this assumption.

On the experimental side, measurements of the contact angle performed up to now have provided controversial results. The first experimental determination of the contact angle of $^4$He on Cs system, and its temperature dependence, has been deduced from the force exerted on two parallel plates forming a capillary. Klier, Stefanyi, and Wyatt[6] measured the reduction in pressure $\delta P$ due to the immersion of an array of equally spaced parallel tungsten plates coated with Cesium into liquid $^4$He. Using Young's equation this pressure reduction can be written in terms of the contact angle as $\delta P\propto 2\sigma_{lv}\cos(\theta)/d$, where $d$ is the distance between the plates. This relation allows for a determination of $\theta$. The extrapolation to $T=0$ of the contact angle measured in this way gives $\theta=48°$.[6] This value has been confirmed recently by a new experiment by the same group.[13]

A smaller value of $\theta=25°$ has later been obtained by means of direct optical measurement using interferometric techniques.[14]

Recently macroscopic droplets of superfluid $^4$He on a Cs surface have been observed,[9] and the contact angle directly deduced from visual inspection and estimated to be $\theta\sim 32°$, independently on the droplet size. However, an extremely hysteretic behavior of the contact angle has been found, i.e., different values of $\theta$ are observed, depending on whether the contact line is advancing or receding. Although a common explanation of contact-angle hysteresis attributes it to heterogeneities of the substrate, which acts as pinning centers for the fluid-vapor interfaces, the experimental evidence reported in Ref. 9 seems to exclude this effect, leaving the strong hysteretic behavior unexplained.

We report here theoretical calculations of the $T=0$ structure of liquid $^4$He droplets of different sizes on an ideal, flat surface the binding potential of which is chosen to represent the adsorption properties of a Cs substrate, where ''dry'' non-wetting behavior of $^4$He at low temperature is expected.

 

They are performed within a density functional (DF) approach which has been proposed a few years ago to describe the structural and dynamical properties of liquid $^4$He at $T=0$. Due to the computational cost our calculations are limited to rather small sizes, i.e., we consider microscopic droplets containing up to $N=2500$ $^4$He atoms. We supplement our computations with analytical calculations, based on a simple ansatz for the shape of the adsorbed droplets, which helps to relate our results for microscopic droplets to the experimental measurements of the contact angle of macroscopically thick films/droplets. A comparison with these experimental results is also presented, giving a semiquantitative agreement with measured contact angles.

## II. COMPUTATIONAL METHOD

We describe the properties of superfluid $^4$He at $T=0$ in terms of the total-energy functional proposed in Ref. 15. This functional is an extension of a previous phenomenological one,[16] which has been extensively used to study static and dynamical properties of inhomogeneous phases of liquid $^4$He (surfaces, droplets, films, etc.). The functional of Ref. 16 is known to give a good description of the $T=0$ equation of state, of the static density-density response function of the bulk liquid and of the properties of the free surface of liquid $^4$He. It has been used in a variety of calculations, ranging from the study of impurities[17] and electrons[18] in bulk $^4$He, to alkali atom adsorption on the surface of liquid $^4$He (Ref. 19) and wetting phenomena on alkali-covered substrates.[21] In Ref. 15 this functional has been supplemented by an extra term depending on the gradient of the liquid density and it now correctly reproduces the static structure factor and the bulk dispersion relations of sound excitations in liquid $^4$He. This extended functional has been applied to the study of density oscillations in $^4$He clusters,[22] of surface excitations in $^4$He films[15,23] and of other related dynamical phenomena.[20]

The static properties of unsupported, spherical $^4$He clusters have also been studied,[20] with results in extremely good agreement with state-of-the-art quantum Monte Carlo calculations. In view of this agreement, we believe that the density-functional description should be accurate enough to allow for quantitative predictions in the case under study here.

According to Ref. 15 the static properties of liquid $^4$He at $T=0$ are described by the energy density functional:[24]

$$E_{\mathrm{He}}[\rho(\mathbf{r})]=\frac{\hbar^2}{2M}\int d\mathbf{r}[\nabla\rho^{1/2}(\mathbf{r})]^2+\frac{1}{2}\int d\mathbf{r}\int d\mathbf{r}'\,\rho(\mathbf{r})\times\rho(\mathbf{r}')V_{\diagup}(|\mathbf{r}-\mathbf{r}'|)+\frac{c_2}{2}\int d\mathbf{r}\rho(\mathbf{r})(\overline{\rho_{\mathbf{r}}})^2+\frac{c_3}{3}\int d\mathbf{r}\rho(\mathbf{r})(\overline{\rho_{\mathbf{r}}})^3+\frac{\hbar^2}{4M}\alpha_s\int d\mathbf{r}\times\int d\mathbf{r}'F(\mathbf{r}-\mathbf{r}')\left(1-\frac{\rho(\mathbf{r})}{\rho_{0s}}\right)\nabla\rho(\mathbf{r})\times\nabla\rho(\mathbf{r}')\left(1-\frac{\rho(\mathbf{r}')}{\rho_{0s}}\right). \tag{2}$$

Here $\rho(\mathbf{r})$ is the density of liquid $^4$He and $M$ is its atomic mass. The first term is the quantum kinetic energy, the second contains a two-body $^4$He-$^4$He pair potential $V_{\diagup}(r)$ screened at distances shorter than a characteristic length $h_{\diagup}$, while the third and the fourth terms (correlation terms) which contain $\overline{\rho_r}$, i.e., the average of the density over a sphere of radius $h_{\diagup}$, account for the internal kinetic energy and for the increasing contribution of the hard-core He-He repulsion when the density is increased. The last term contains the gradient of the density at different points and corresponds to a nonlocal correction to the kinetic energy. The free parameters $h_{\diagup}, c_2, c_3$, are adjusted in order to reproduce the experimental values of the density, of the energy per atom, and of the compressibility for bulk liquid $^4$He at zero pressure, while the width $l$ of the gaussian function $F$ and the parameters $a_s$ are fixed to reproduce the peak of the static response function in bulk liquid. The parameter $\rho_{0s}$ is finally fixed to ensure an accurate pressure dependence of the response function. For a detailed description of the various terms and their numerical values as well, we refer the reader to Ref. 15.

To include the interaction with the substrate, we use a binding potential $V_s(z)$ which accounts phenomenologically for the interaction between Cs, occupying the half space $z\leqslant 0$, and one $^4$He atom located at a distance $z$ above the surface, which is taken to be ideally flat. We do not include any corrugation of the surface on the atomic scale to mimic its actual electronic distribution. This is a very good approximation for the case of $^4$He adsorption on a Cs surface, where the experiments[25] indeed indicate that a surprisingly smooth surface is seen by the $^4$He atoms.

The physisorption potential $V_s(z)$ is taken in the form originally proposed in Ref. 26, as a sum of a Hartree-Fock repulsion term and a van der Waals attraction:

$$V_s(z)=V_0(1+\alpha z)e^{-\alpha z}-f_2(\beta(z)(z-z_{vdw}))\frac{C_3}{(z-z_{vdw})^3}. \tag{3}$$

Here $z_{vdw}$ is the position of the image plane while the Hamaker's constant $C_3$ determines the strength of the van der Waals long-range attractive part. The damping function is given by $f_2(x)=1-e^{-x}(1+x+x^2/2)$, and the damping parameter is $\beta(z)=\alpha^2 z/(1+\alpha z)$. Very reliable values for the parameters entering Eq. (3) and describing the interaction of $^4$He with alkali substrates have been calculated from first principles.[27] We quote here the values appropriate to a Cs substrate, used in our calculations: $V_0=0.1405$ eV, $\alpha=0.9370a_0^{-1}$, $C_3=0.5793$ eV $a_0^3$, $z_{vdw}=0.3623a_0$. The resulting potential $V_s$ has a minimum of $D=0.601$ meV at $z_0=8.61a_0$.

The total energy functional of liquid $^4$He interacting with a Cs surface is thus:

$$E[\rho(\mathbf{r})]=E_{\mathrm{He}}[\rho(\mathbf{r})]+\int d\mathbf{r}\rho(\mathbf{r})V_s(\mathbf{r}). \tag{4}$$

We determine the optimal, minimum-energy shape of a $^4$He droplet adsorbed on the surface by a direct minimization

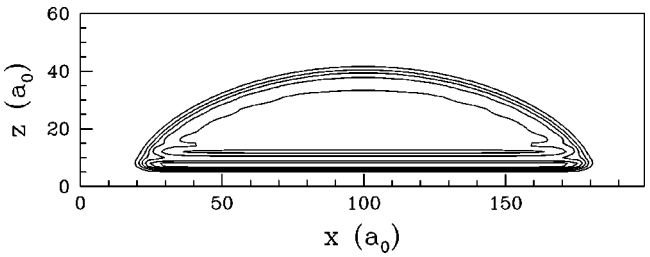


FIG. 1. Contour plot showing the droplet density for the case $N=1500$.

of the above functional with respect to density variations. Given the very small dimensions of our droplets, gravitational effects are neglected in our study. No geometrical or symmetry constraints are imposed during the minimization and the droplet is allowed to find its lowest-energy structure by full relaxation. The minimum-energy principle, subject to the constraint of a constant number of $^4$He atoms:

$$\int d\mathbf{r}\rho(\mathbf{r})=N, \tag{5}$$

leads to the Euler-Lagrangian equation:

$$\left(-\frac{\hbar^2}{2M}\nabla^2+U[\rho(\mathbf{r})]\right)\sqrt{\rho(\mathbf{r})}=\mu\sqrt{\rho(\mathbf{r})}, \tag{6}$$

where the effective potential $U$ is defined as $U[\rho(\mathbf{r})] \equiv \delta E[\rho(\mathbf{r})]/\delta\sqrt{\rho}$ and $\mu$ is a Lagrange multiplier the value of which is fixed by the normalization condition Eq. (5).

In our calculations we used a supercell geometry, with periodic boundary conditions imposed on the $^4$He wave function $\Psi(\mathbf{r})\equiv\sqrt{\rho(\mathbf{r})}$ and on the $^4$He density $\rho(\mathbf{r})$ itself. Both $\Psi$ and $\rho$ are expanded in plane waves, the maximum number of which is chosen such as to give converged values for the total energy of the system and for the structural parameters of the droplets. The self-consistent iterative solution of the Euler-Lagrange equation [Eq. (6)] provides the extremal density profile $\rho(\mathbf{r})$ of the droplet. The computational method used for the functional minimization of the total-energy equation (4) is described in Ref. 18, to which the reader is referred for further details.

We treated droplets containing different numbers of atoms $N$: 100, 300, 600, 1000, 1500, and 2500. In each case the supercell size was chosen large enough to decouple the droplet from its repeated images. As a starting configuration we usually assumed a spherical cluster placed close to the surface plane, which was then allowed to freely relax towards its minimum-energy configuration.

## III. NUMERICAL RESULTS

A typical density profile obtained from the minimization of the density functional equation (4) is shown in Fig. 1, where the minimum-energy $^4$He density distribution for a droplet composed of $N=1500$ atoms is shown with a contour plot. The origin of the vertical $z$ axis is chosen at the position of the image plane $z_{vdw}$ [see Eq. (3)], which in the following will be referred to as the Cs surface plane position.

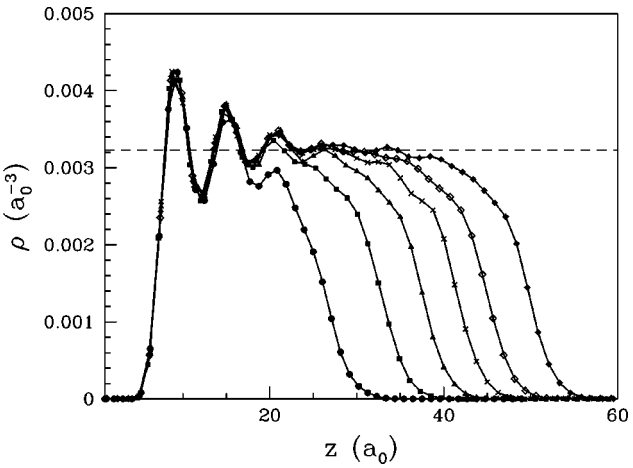


FIG. 2. $^4$He density profiles along a line passing through the top of the droplet and perpendicular to the surface plane, for different sizes of the droplets: $N=100$ (dots), $N=300$ (squares), $N=600$ (triangles), $N=1000$ (crosses), $N=1500$ (open diamonds), and $N=2500$ (filled diamonds). The point $z=0$ is the position of the Cs surface plane.

The density profiles for the various droplets with different $N$ are shown in Fig. 2, where the $^4$He density along the line passing through their center is plotted as a function of the distance $z$ from the surface plane. Note the marked oscillations of the density around its bulk value $\rho_0$ (shown with a dashed line) close to the Cs surface, which show a tendency of the liquid to develop ''layers.'' The droplet density $\rho$ decreases rapidly to zero on the solid surface side due to the presence of the steep repulsive part of the He-surface potential [Eq. (3)], whereas the liquid surface is more diffuse towards the liquid-vacuum side.

Figure 3 shows, with solid and dotted lines, respectively, the contour plots of the cross sections of various droplets at two different values of the density, $\rho=\rho_0/2$ and $\rho=\rho_0/10$, respectively.

A clear feature that emerges from these profiles is that the local structure close to the surface, where the ''layered''

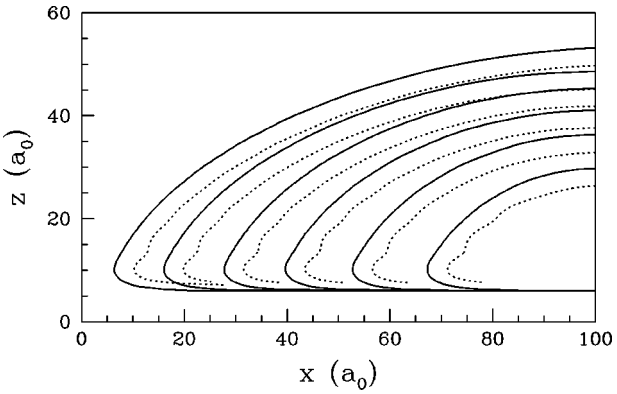


FIG. 3. Droplet cross sections at $\rho=\rho_0/10$ (solid lines) and $\rho=\rho_0/2$ (dotted lines), from $N=100$ (innermost sections) to $N=2500$ (outermost sections).

structure develops, is independent on the droplet size. This region can be identified with the ''core'' of the contact line,[28] where the deviations from the average density of an adsorbed film/droplet are usually confined.

We note in passing that the linear dimension of the core region in Fig. 3 is of the same order of magnitude of the core thickness $\zeta_c$ as defined in Ref. 28, $\zeta_c \sim a_c/\theta$, where $a_c \sim (C_3\rho/\sigma)^{1/2}$ and $\theta$ is the contact angle. For the $^4$He-Cs system $a_c \sim 15a_0$. By taking $\theta \sim 30-40°$, one finds $\zeta_c \sim 30a_0$

In order to define unambiguously the contact angle formed by the droplet with the Cs substrate, one must first define the surface of the droplet. For all droplets we take a circular ''base,'' of radius $R_{max}(N)$, located a distance $z_0$ above the solid as the surface on the solid side. On the vapor side, we use the Gibbs surface, i.e., the surface that encloses the correct number of atoms if the density is uniform and its value equal to the bulk liquid density.

Mathematically the Gibbs surface is defined by

$$\zeta(\mathbf{R}) = \frac{1}{\rho_0}\int_0^\infty dz\,\rho(\mathbf{R},z) + z_0 . \tag{7}$$

Here $\mathbf{R}$ is the two-dimensional vector along the surface plane and $z_0$ corresponds to the position where the substrate potential $V_s(z)$ attains its minimum, i.e., is the position of the first ''layer'' of He atoms in the droplet. The closed surface enclosing the droplet is obtained by intersecting $\zeta(\mathbf{R})$ with the ''base'' of the droplet.

Even in the presence of quite large deviations from the bulk density that occur close to the substrate plane (see Fig. 2), this definition of the droplet surface is meaningful and accurate. This can be checked by defining a ''surface'' energy contribution $E_s$, which can be extracted from the results of our calculations according to the definition

$$E_s = E(N) - \mu_0 N - \int d\mathbf{r}\,\rho(\mathbf{r})V_s(\mathbf{r}). \tag{8}$$

Here $E(N)$ is the total-energy functional [Eq. (4)] calculated in correspondence of the extremal density $\rho(\mathbf{r})$ for a given $N$, while $\mu_0 = -7.16$ K is the energy per $^4$He atom in the bulk liquid, calculated with the same supercell and energy cutoff used for the droplet calculations.

By assuming $E_s = \sigma A$, where $\sigma$ is the liquid-vapor surface tension and $A$ is the total area of the Gibbs surface as defined above, we find values of $\sigma$ ranging from 0.26 Å K to 0.27 Å K, depending on the size of the droplet. Within the accuracy of our calculations, these values agree with the experimental value $\sigma = 0.274$ Å K. Although small variations of $\sigma$ are expected for differently curved surfaces (i.e., for droplets with different sizes), we do not anticipate any quantitative conclusion about this effect, given the finite accuracy of our calculations.

## IV. CLASSICAL MODEL

Starting from a simplified model of droplet adsorption on an ideal flat surface, in this section we derive some results that will be helpful in the following to define a contact angle for our calculated droplet profiles.

Specifically, we assume that the liquid-vapor interface is abrupt, i.e., the density of the droplet is taken to be equal to the bulk density of the liquid $\rho_0$, whereas $\rho = 0$ identifies the vapor side. We consider a droplet of a purely classical fluid, with surface tension and bulk density values appropriate to $^4$He ($\sigma = 0.274$ K Å$^{-2}$ and $\rho_0 = 0.0218$ Å$^{-3}$).

If the droplet is enclosed by a circular ''base'' of radius $R_{max}$ at $z_0$ on the solid side, and by the surface $\xi(\mathbf{R})$ on the vapor side, then its energy may be written as

$$E_d = \sigma\left(\int d\mathbf{R}\sqrt{1+(\nabla\xi(\mathbf{R}))^2} + \pi R_{max}^2\right) + \rho_0\int d\mathbf{R}\int_{z_0}^{\xi(\mathbf{R})} dz\,V_s(z). \tag{9}$$

The actual shape $\xi(\mathbf{R})$ will be such as to satisfy the normalization condition:

$$\rho_0\int d\mathbf{R}\int_{z_0}^{\xi(\mathbf{R})} dz = N, \tag{10}$$

minimizing, at the same time, the droplet energy $E_d$.

### A. The ellipsoidal cap model

Before trying to solve the Euler-Lagrange equation obtained by a direct minimization of Eq. (9), we start with an educated guess for the analytic form of the equilibrium shape of the droplet, depending on some adjustable parameters, and determine these parameters by the variational principle $\delta E_d = 0$. Despite the restriction imposed by the choice of the analytic form of the droplet profile, this approach has the advantage that the relevant structural properties of the droplet can be analytically determined for any $N$.

As the simplest *ansatz*, we assume that an adsorbed droplet exhibits cylindrical symmetry around the $z$ axis, and that its shape is that of an ellipsoid of semiaxis $b$ along $z$ and $b/e$ parallel to the surface, centered at the position $[0,0,-(h-b)]$ and cut by a plane located a distance $z_0$ above the substrate.

We determine variationally the parameters $b$, $h$, and the eccentricity $e$ by minimizing the total energy of such a droplet in the presence of the substrate potential $V_s(z)$. Despite its simplicity, this ellipsoidal cap model (ECP) shares a number of features with the more realistic results obtained from our density-functional calculations, and as shown in the following, it proves to be helpful in clarifying those results.

To simplify this model still further, the substrate potential is taken to be[21]

$$V_s^{LJ}(z) = \frac{4C_3^3}{27D^2z^9} - \frac{C_3}{z^3} \tag{11}$$

where, as usual, $C_3$ is the Hamaker's constant and $D$ gives the well depth.

While keeping the essential physical features of the potential (3) actually used in our DF calculations, i.e., the same long-range tail, well depth, and minimum position, this potential has a simpler analytical form and thus it is more manageable when included in model calculations. For example,

the position $z_0$ of the base of the ellipsoidal cap, taken as the position of the minimum of $V_s^{LJ}(z)$, can be written explicitly as $z_0=(2C_3/3D)^{1/3}\sim 8.61a_0$.

From Eq. (9) one sees that the total energy of this cap is the sum of the energy $\sigma A(b,h,e)$ required to form the total surface $A(b,h,e)$ of the cap, and of a volume term $\rho_0\int dV(b,h,e)V_s^{LJ}(z)$, which takes into account the interaction with the Cs surface. By imposing the requirement of a fixed number of particles $N=\rho_0\int dV(b,h,e)$, the total energy (9) becomes a function of only two parameters, which we chose to be $h$ and $e$. We then perform analytically the minimization of the total energy with respect to these two parameters and find the equilibrium profile for a given $N$.

We postpone the discussion of the ECM results to the following section, where they will be compared with those of DF calculations.

At this point we only remark that the eccentricity $e$ for the minimum-energy ellipsoidal cap is found to reach a maximum value of about 2 when $N\sim 10^5$ atoms, and then it decreases monotonically to $e=1$ as $N\to\infty$, i.e., a spherical cap is recovered as the limiting shape of an adsorbed *macroscopic* droplet in our model. It is thus interesting to discuss at some length the $N\to\infty$ limit of the ECM, that is, the case of a spherical cap.

Since $e=1$ in this case, only one parameter (which we choose to be $h/z_0$) must be variationally determined, the other being fixed by the normalization condition (10).

Minimization of the total energy with respect to this variational parameter leads to the following equation for $t\equiv h/z_0$:

$$\left(\frac{11}{12}-4C\right)t^8-\frac{83}{42}t^7+\frac{43}{42}t^6+\frac{1}{42}(t^5+t^4+t^3+t^2+t)-\frac{1}{12}=0 \tag{12}$$

where the adimensional parameter

$$C\equiv\frac{\sigma}{\rho}\left(\frac{12}{27C_3D^2}\right)^{1/3} \tag{13}$$

characterizes the adsorption properties of the spherical cap onto the surface. As long as $C$ remains smaller than $C_0=11/48$, then the height of the droplet $h$ satisfying Eq. (12) remains finite (i.e., since $N\to\infty$, the droplet covers the whole surface with a microscopically thin film separating the substrate from the vacuum), whereas as $C\to C_0$ the film thickness diverges. We interpret this as the onset of the nonwetting-to-wetting regime for our simple model. We note that the condition $C\geqslant C_0$ for the nonwetting-to-wetting transition is the same as that obtained in Ref. 29 by comparing the gain in potential energy on producing a thick film delimited by two planar, infinitely extended surfaces with the cost in energy (per unit area) due to the surface tension:

$$2\sigma_{lv}\geqslant-\rho_0\int_{z_0}^{\infty}dz\,V_s(z). \tag{14}$$

This approximate criterion has been found to be consistent with $T=0$ density-functional calculations for a planar, infinitely extended film on a surface.[3] By inserting the form Eq. (11) for $V_s$ into Eq. (14) and integrating, one immediately finds the condition $C\geqslant 11/48$ obtained for the case of a spherical cap.

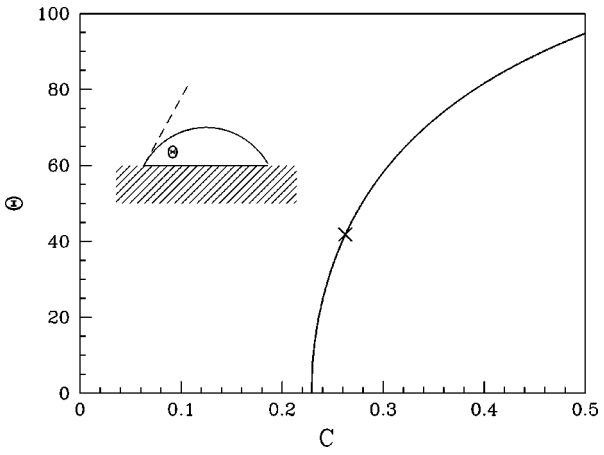


FIG. 4. Contact angle $\Theta$ of a spherical cap shown as a function of the coupling constant $C$ (defined in the text). The cross identify the contact angle for $C=C_{\text{He-Cs}}$.

Thus even in the presence of the constraint of fixed geometrical shape a unique, although approximate, criterion for nonwetting can be obtained both for macroscopic drops and planar films, i.e., the geometrical constraints that we impose in our ellipsoidal cap model are not so stringent.

When $C\geqslant C_0$ we can define a geometric contact angle $\Theta$ of the macroscopic spherical droplet as the angle between the tangent to the drop profile and the substrate at the point of contact. The contact angle can be easily found from the equilibrium value of $h$, and it turns out to be

$$\cos\Theta=\frac{11-24C}{24C}. \tag{15}$$

The contact angle $\Theta$ is shown in Fig. 4 as a function of the coupling constant $C$. If we insert the values appropriate for the $^4$He-Cs system[27] into Eq. (13), we find $C=0.2627$, which determines a contact angle $\Theta=42°$ for a macroscopically thick droplet, as shown in Fig. 4.

At this point we note from Fig. 4 that the value of $C$ appropriate to the $^4$He-Cs system lies in a region where small changes in the value of $C$ result in substantial variations of $\Theta$. One must thus be aware that even a small inaccuracy in the determination of the potential parameters $C_3$ and $D$ will affect the value of $C$ and thus produce significant changes in the limiting value for the contact angle of the spherical cap model.

### B. Exact minimization

We now go back to Eq. (9) and derive some general, exact results for the shape $\xi(\mathbf{R})$ of the adsorbed droplet.

It is immediately apparent that mimization of $E_d$ with respect to $\xi$ leads to a Euler-Lagrange equation that may be written as

$$\rho V_s(\xi(\mathbf{R}))-\sigma H(\xi(\mathbf{R}))=\text{const}, \tag{16}$$

where $H(\mathbf{R}) \equiv \vec{\nabla} \cdot \vec{\nabla} \xi(\mathbf{R}) / \sqrt{1+[\nabla \xi(\mathbf{R})^2]}$ is the mean curvature of $\xi$ at $\mathbf{R}$. The constant, which we will write as $-\lambda\rho$ in the following, is determined by the condition that the number of atoms in the droplet, i.e., its volume, is fixed.

This remarkable relation for the shape of simple fluids near rigid solids was first derived by Berry[30] from a statistical mechanics analysis using a simple approximation for the pair-correlation function of the liquid and thus its validity goes beyond that of Eq. (9). Its limits may be found in Berry's discussion.

For simplicity, let us consider the one-dimensional analog of Eq. (16) so that now $\xi(x)$ indicates the height of the droplet profile measured from the position of the flat surface plane with $x$ a Cartesian coordinate along that plane, while we assume translational symmetry along the $y$ direction. The curvature can thus be written as $H(x) = -\xi''/(1+\xi'^2)^{3/2}$, and Eq. (16) becomes

$$\frac{\sigma \xi''}{(1+\xi'^2)^{3/2}} - \rho V_s(\xi) + \lambda\rho = 0, \tag{17}$$

which admits a first integral in the form

$$\frac{\sigma}{(1+\xi'^2)^{1/2}} - \lambda\rho\xi + \rho P(\xi) = K, \tag{18}$$

where $K$ is a constant and $P(\xi) \equiv -\int_{\xi}^{\infty} dz' V_s(z')$.

By considering the balance of the horizontal forces acting on a portion of the fluid near the contact line, it can be shown[28] that $K = \sigma - S$, where $S = \sigma_{so} - \sigma_{sl} - \sigma$ is the so-called spreading coefficient. At this point the contact angle $\theta_e$ can be introduced through Young's equation $-K = \sigma \cos\theta_e$ and Eq. (18) becomes

$$\cos\theta_e = \cos\theta(\xi(x)) + \rho P(\xi(x))/\sigma - \lambda\rho\xi(x)/\sigma, \tag{19}$$

where $\theta(\xi(x))$ is the angle formed by the tangent to $\xi$, at the position $x$, with the $x$ axis. If we measure $h$, the maximum height of the droplet above the surface plane, at the position where $\xi' = 0$, and the corresponding radius of curvature at the apex of the droplet, $R_c = |\xi''|^{-1}$, then we can use Eq. (17) to evaluate $\lambda$ and substitute its value into Eq. (19) to get

$$\cos\theta_e = 1 + \rho P(h)/\sigma - \rho V_s(h) h/\sigma - h/R_c. \tag{20}$$

This relation gives the contact angle $\theta_e$ in terms of the substrate potential and of the two structural parameters of the droplet $h$ and $R_c$. For *macroscopic* droplets $h \to \infty$ and both $P(h)$ and $V_s(h)$ are negligibly small. In this limit one has

$$h = R_c(1 - \cos\theta_e). \tag{21}$$

In the case of macroscopic droplets $\theta_e$ may be identified with the geometrical contact angle at the three-phase contact line: the above equation may be read as simply relating the radius $R_c$ and the height $h$ of a *spherical* cap on the surface. Once again we recover the result that, as long as gravitational effects may be neglected, the limiting shape of a macroscopic droplet resting on an attractive substrate is spherical in shape.

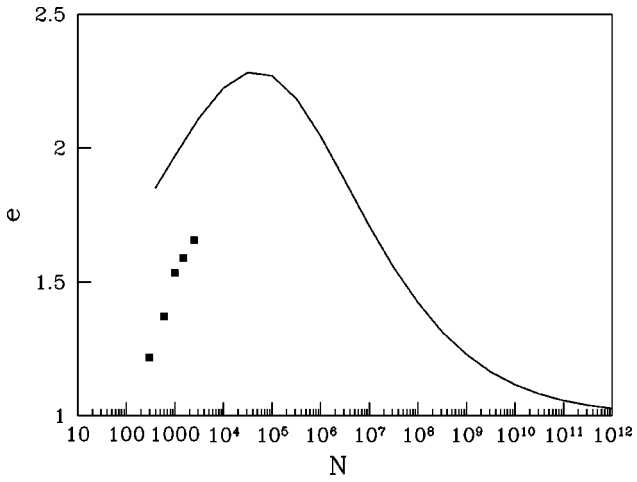


FIG. 5. Eccentricity of the ellipsoidal cap as a function of the number of atoms in the droplet. The filled squares show the results of our DF calculations, the solid line shows the ECM results.

## V. DISCUSSION

We compare in this section our density-functional results described in Sec. III with the predictions of the classical model described in the previous section.

As a starting point we checked whether the actual profile $\zeta(\mathbf{R})$ of the droplets obtained through Eq. (7) from our DF calculations, could indeed be approximated by an ellipsoidal profile.

We thus fitted our calculated Gibbs surfaces with an ellipsoidal cap, determining for each droplet three parameters, the height $h$, the semiaxis $b$, and the eccentricity parameter $e$, which give the best fit to our calculated surfaces. We verified that the root mean deviation of the calculated surfaces from the fit is always smaller than 0.1%, at least in the region not too close to the Cs surface. Deviations from the analytical fit actually occur at distances from the surface comparable with the core linear dimension $a_c$ defined in Sec. III.

The calculated values of the eccentricity $e$ resulting from our fitting procedure are shown in Fig. 5 with squares, while in Fig. 6 we report the maximum height $h$ of our DF droplets. In both figures the solid lines show the corresponding ECM predictions. We notice that, although both figures indicate that DF droplets are more elongated than predicted by the ECM model, the values of the aspect ratio (which is defined as the ratio $h/2R_{max}$) are very similar in the two calculations, as shown in Fig. 7, especially for the larger $N$ we calculated.

This may suggest to extrapolate our DF results to large $N$, where the aspect ratio of the ECM model for macroscopic spherical droplets takes the value 0.19 (shown by the dashed line in Fig. 7).

We may check on the validity of the classical model described in Sec. IV by inserting the Gibbs profile $\zeta(\mathbf{R})$ obtained from our DF calculation through Eq. (7) into the right-hand side of Eq. (19). As shown in Fig. 8, where the right-hand side, call it $F(\zeta)$, is plotted as a function of $\zeta$ for various $N$, one sees that indeed, as $\zeta$ increases, $F$ becomes a constant, as required by Eq. (19) for the profiles minimizing the droplet energy $E_d$.

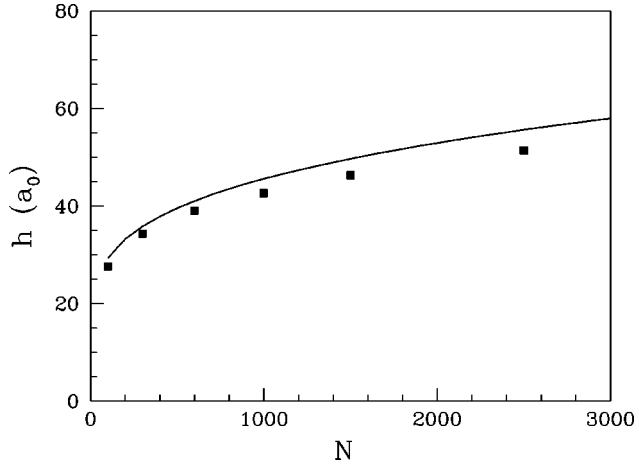


FIG. 6. Droplet height as a function of size: filled squares are the results of density-functional calculations, the solid line shows the ECM results.

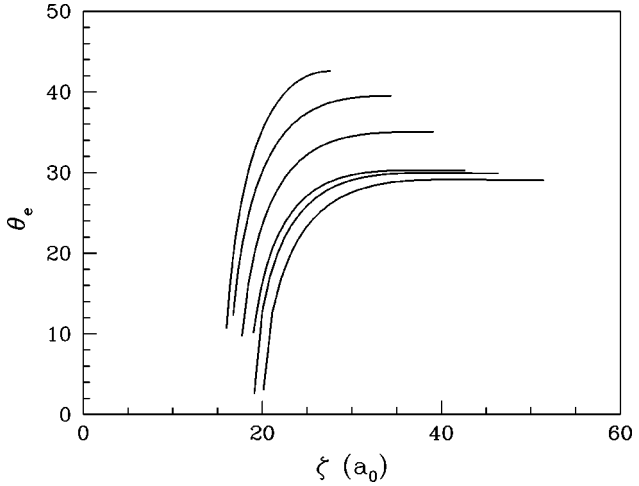


FIG. 8. Right-hand side of Eq. (19) as a function of the vertical position along the droplet DF profile, for the different values of $N$ from $N=100$ (uppermost curve) to $N=2500$ (lowest curve).

We interpret this finding as a check on the adequacy of the classical model to describe the results of the DF calculation, and at the same time as the definition of the ''core'' region as the region where $F$ is rapidly increasing. Physically it corresponds to the portion of the droplet close to the surface, where its density exhibits the layered structure (see Fig. 2) and therefore is far from being uniform. As the mathematical definition of this region, we will call ''core'' the portion of the droplet with $z_0 \leqslant z \leqslant \zeta_0$, with $\zeta_0$ defined by the condition $|dF(\zeta)/d\zeta|_{\zeta_0}=1$.

At this point we can finally define the contact angle as the geometrical contact angle measured in the region just outside the core region, i.e., for $\zeta \geqslant \zeta_0$. The calculated contact angle at $\zeta_0$ are shown in Fig. 9 (with squares) as a function of $N$. The ECM results are also reported for comparison. It appears that the contact angle defined in this way is almost independent on the droplet size. Actually this is apparently true only in the narrow region of $N$ values shown in the figure, which encompasses our calculated droplet sizes. In the limit $N \to \infty$ of macroscopically thick droplets the contact angle predicted by the ECM tends toward the value $\Theta=42\,^\circ$ for a spherical cap, as discussed in Sec. V. This limiting value is shown in Fig. 9 with a dashed line.

The behavior of the results shown in Fig. 9 for the values $\theta(N)$ obtained from DF calculations and from the ECM model, i.e., an almost constant difference between the two as $N$ increases, suggests an extrapolation for the macroscopic contact angle, even if we cannot predict the DF value of $\theta$ for very large droplets.

Under the reasonable assumption that the same constant difference as in Fig. 9 would be obtained for larger values of $N$, we would predict in this way a value of $\theta_\infty \sim 36\,^\circ$, which is in reasonable agreement with the value measured in Ref. 9, and in between the two values measured in Refs. 14 and 6.

Instead of defining the contact angle as done above, i.e., as the geometrical contact angle at $\zeta_0$, we could choose the alternative approximation of inserting our DF profiles $\zeta(R)$ in place of $\xi(x)$ into Eq. (19) and take as the contact angle

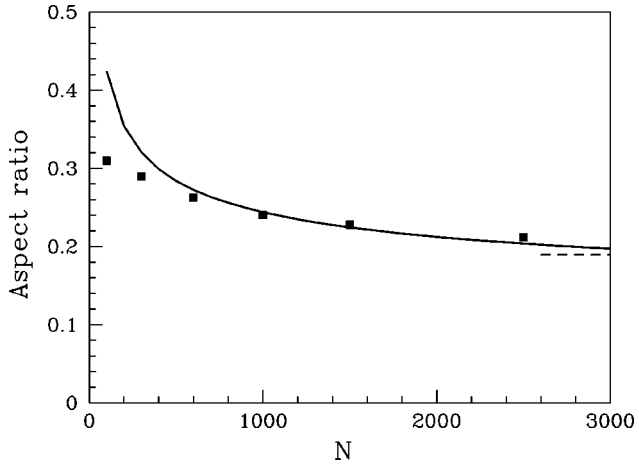


FIG. 7. Aspect ratio as a function of size: filled squares are the results of density-functional calculations, the solid line shows the ECM results. The dash-dot line shows the $N \to \infty$ limit, where the shape of a spherical cap is recovered.

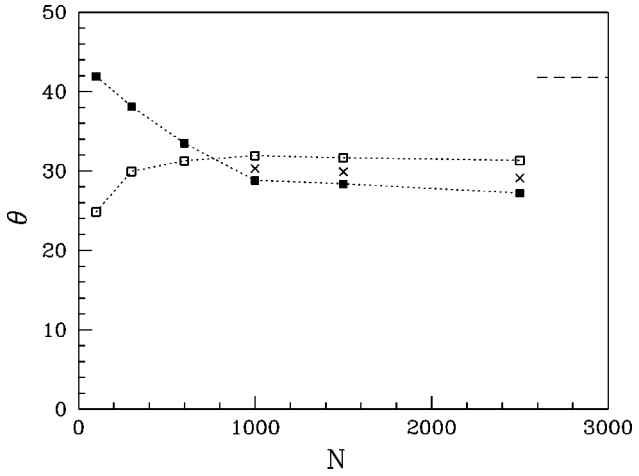


FIG. 9. Contact angle from DF calculations (filled squares) and ECM (open squares). The DF results are obtained as explained in the text. The crosses show the values of $\theta_e$ as obtained from Eq. (19) in the region where $\theta_e$ is constant. The dash-dot line shows the $N \to \infty$ limit, where a spherical cap is the preferred shape.

the value of $\theta_e$ in the outer region, where it becomes constant. The results obtained in this way, which are shown with crosses in Fig. 9, do not differ very much from the geometrical contact angles at $\zeta_0$ (filled squares in Fig. 9), so that by means of the same extrapolation procedure, we would come to almost the same value for the macroscopic contact angle. Of course, by using Eq. (19), we are assuming that the fact that the contact line is not straight, i.e., that the droplet is not one dimensional, is not important. Corrections due to curvature of the contact line and to the curvature dependence of the surface tension would correspond to additional terms in Eq. (9) and become negligible as $N$ increases. We checked that their effect on the contact angle is negligible as soon as $N \geqslant 1500$ by making a complete DF calculation for a pancake geometry[28] of the adsorbed liquid, i.e., by assuming translational symmetry along the $y$ axis.

## VI. SUMMARY

In summary, by using a density-functional approach, we have calculated the $T=0$ structure of liquid $^4$He droplets on a Cs surface, where ''dry'' nonwetting behavior of $^4$He is expected. We described the microscopic structure of the liquid droplets in the vicinity of the core of the contact line. With the help of a classical model we have defined a ''core region'' and a contact angle for microscopic droplets. We have also discussed a minimum-energy configuration for droplets having the shape of an ellipsoidal cap. This ''ellipsoidal cap model,'' which may be extended to drops of any size, allows us to extrapolate the contact angle from our microscopic DF calculation to the value appropriate to macroscopic drops, $\theta_\infty = 36°$. This value is close to the experimental determination $\theta \sim 32°$ of Ref. 9, and larger (smaller) by $\sim 10°$ than the experimental values of Ref. 14 (Ref. 6).

We conclude by underlining two possible sources of inaccuracy in our results. The first is that, as explained in Sec. IV, the value for the contact angle of the spherical cap, which we use to extrapolate our DF results to the limit of macroscopic droplets, is rather sensitive to any inaccuracy in the determination of the adimensional parameter $C \equiv (\sigma/\rho)(12/27C_3D^2)^{1/3}$, i.e., in the determination of the $^4$He-substrate potential parameters. Moreover, our calculations are appropriate to zero temperature, while experiments are of course done at finite, albeit small, $T$. A reduction of the contact angle with temperature, with respect to its $T=0$ value, should thus be taken into account. Further work is in progress aimed at understanding the nature of surface excitations at the solid-liquid interface and their role in the temperature dependence of the solid-liquid surface tension.

## ACKNOWLEDGMENTS

We acknowledge useful discussions with G. P. Mistura and E. Rolley.

[1] B. Evans and M. Chan, Phys. World **4**, 48 (1996).
[2] E. Cheng, M. W. Cole, W. F. Saam, and J. Treiner, Phys. Rev. Lett. **67**, 1007 (1991).
[3] E. Cheng, M. W. Cole, W. F. Saam, and J. Treiner, Phys. Rev. **46**, 13 967 (1992).
[4] P. J. Nacher and J. Dupont-Roc, Phys. Rev. Lett. **67**, 2966 (1991).
[5] J. E. Rutledge and P. Taborek, Phys. Rev. Lett. **69**, 937 (1992).
[6] J. Klier, P. Stefanyi, and A. F. G. Wyatt, Phys. Rev. Lett. **75**, 3709 (1995).
[7] P. Stefanyi, J. Klier, and A. F. G. Wyatt, Phys. Rev. Lett. **73**, 692 (1994).
[8] D. Ross, P. Taborek, and J.E. Rutledge, Phys. Rev. Lett. **74**, 4483 (1995).
[9] D. Ross, J. E. Rutledge, and P. Taborek, Science **278**, 664 (1997).
[10] K. R. Atkins and Y. Narahara, Phys. Rev. **138**, A437 (1965).
[11] P. Taborek and J. E. Rutledge, Phys. Rev. Lett. **68**, 2184 (1992).
[12] M. S. Pettersen and W. F. Saam, J. Low Temp. Phys. **90**, 159 (1993).
[13] J. Klier and A. F. G. Wyatt, J. Low Temp. Phys. **110**, 919 (1998).
[14] E. Rolley and C. Guthmann, J. Low Temp. Phys. **108**, 1 (1997).
[15] F. Dalfovo, A. Lastri, L. Pricaupenko, S. Stringari, and J. Treiner, Phys. Rev. B **52**, 1193 (1995).
[16] J. Dupont-Roc, M. Himbert, N. Pavloff, and J. Treiner, J. Low Temp. Phys. **81**, 31 (1990).
[17] F. Dalfovo, Z. Phys. D **29**, 61 (1994).
[18] F. Ancilotto and F. Toigo, Phys. Rev. B **50**, 12 820 (1994).
[19] F. Ancilotto, E. Cheng, M. W. Cole, and F. Toigo, Z. Phys. B **98**, 323 (1995).
[20] F. Dalfovo, A. Fracchetti, A. Lastri, L. Pitaevskii, and S. Stringari, Phys. Rev. Lett. **75**, 2510 (1995); J. Low Temp. Phys. **104**, 367 (1996).
[21] E. Cheng, M. W. Cole, J. Dupont-Roc, W. F. Saam, and J. Treiner, Rev. Mod. Phys. **65**, 557 (1993).
[22] M. Casas, F. Dalfovo, A. Lastri, L. Serra, and S. Stringari, Z. Phys. D **35**, 67 (1995).
[23] A. Lastri, F. Dalfovo, L. Pitaevskii, and S. Stringari, J. Low Temp. Phys. **98**, 227 (1995).
[24] The complete functional, which includes terms depending on the superfluid velocity $\mathbf{v}_s$, can be found in Ref. 15: since we are only interested here in equilibrium properties where $\mathbf{v}_s = 0$, we use, and quote, the static version of this functional where these terms have been omitted.
[25] J. D. White, J. Cui, M. Strauss, R. D. Diehl, F. Ancilotto, and F. Toigo, Surf. Sci. **307**, 1134 (1994).
[26] E. Zaremba and W. Kohn, Phys. Rev. B **15**, 1769 (1977).
[27] A. Chizmeshya, M. W. Cole, and E. Zaremba, J. Low Temp. Phys. **110**, 677 (1998).
[28] P. G. de Gennes, Rev. Mod. Phys. **57**, 827 (1985).
[29] E. Cheng, M. W. Cole, J. Dupont-Roc, W. F. Saam, and J. Treiner, Rev. Mod. Phys. **65**, 557 (1993).
[30] M. V. Berry, J. Phys. A **7**, 231 (1974).